THE JOURNAL OF BIOLOGICAL CHEMISTRY VOL. 282, NO. 25, pp. 18388–18396, June 22, 2007

Mode of Membrane Interaction and Fusogenic Properties of a *de Novo* Transmembrane Model Peptide Depend on the Length of the Hydrophobic Core*

Received for publication, January 4, 2007, and in revised form, April 24, 2007 Published, JBC Papers in Press, April 24, 2007, DOI 10.1074/jbc.M700099200

Aurélien Lorin[‡1,2], **Benoit Charloteaux**[‡1], **Yael Fridmann-Sirkis**[§], **Annick Thomas**[‡3], **Yechiel Shai**[§4], **and Robert Brasseur**[‡5]

From [‡]*Gembloux Agricultural University, Centre de Biophysique Moléculaire Numérique, B-5030 Gembloux, Belgium and the* [§]*Department of Biological Chemistry, The Weizmann Institute of Science, Rehovot 76100, Israel*

Model peptides composed of alanine and leucine residues are often used to mimic single helical transmembrane domains. Many studies have been carried out to determine how they interact with membranes. However, few studies have investigated their lipid-destabilizing effect. We designed three peptides designated KALRs containing a hydrophobic stretch of 14, 18, or 22 alanines/leucines surrounded by charged amino acids. Molecular modeling simulations in an implicit membrane model as well as attenuated total reflection-Fourier transform infrared analyses show that KALR is a good model of a transmembrane helix. However, tryptophan fluorescence and attenuated total reflection-Fourier transform infrared spectroscopy indicate that the extent of binding and insertion into lipids increases with the length of the peptide hydrophobic core. Although binding can be directly correlated to peptide hydrophobicity, we show that insertion of peptides into a membrane is determined by the length of the peptide hydrophobic core. Functional studies were performed by measuring the ability of peptides to induce lipid mixing and leakage of liposomes. The data reveal that whereas $KALR_{14}$ does not destabilize liposomal membranes, $KALR_{18}$ and $KALR_{22}$ induce 40 and 50% of lipid-mixing, and 65 and 80% of leakage, respectively. These results indicate that a transmembrane model peptide can induce liposome fusion *in vitro* if it is long enough. The reasons for the link between length and fusogenicity are discussed in relation to studies of transmembrane domains of viral fusion proteins. We propose that fusogenicity depends not only on peptide insertion but also on the ability of peptides to destabilize the two leaflets of the liposome membrane.

Biological membranes are a complex mixture of lipids that contain proteins, hydrocarbons, and other constituents (1). In addition, expression, folding, and insolubility problems can make the study of protein-membrane interactions very complicated and limit the results of interpretation (2, 3). Therefore, peptide-membrane interactions are often studied with liposomes of strictly controlled composition (4–8). Use of such model membrane systems also allows one to control the surrounding medium (4). The same principle has been used by several groups with simplified *de novo* model peptides composed of typical residues (9–17). These approaches are useful for analyzing the impact of specific features of peptides and/or membranes on peptide-membrane interactions (12, 18).

The effect of hydrophobicity of TM[6] model peptides on their interaction with membranes has been studied by several groups (16, 19). A threshold of hydrophobicity is required for peptides to be able to insert into membranes and to adopt a transmembrane orientation (19). For example, peptides with a hydrophobic core composed of 24 alanine residues do not adopt a stable transmembrane orientation in phosphatidylcholine-hydrated membranes (15). Lewis *et al.* concluded that this is due to insufficient hydrophobicity rather than poor helicity (15). As a result, TM model peptides are usually composed of a mixture of alanine and leucine residues (16, 20–29). This composition better mimics the mean hydrophobicity of natural TM domains than peptides composed of solely leucine residues (16, 30). Almost all *de novo* TM peptides have aromatic or positively charged residues on either side of the hydrophobic stretch. Lysine and arginine residues are used, since they help to solubilize the peptide, to promote the monomer form, to favor a helical conformation, and to ensure the TM orientation (16, 22). Moreover, it was shown that natural transmembrane α-helices domains are often flanked by lysine and arginine residues (31, 32).

When the length of the hydrophobic stretch of a helical peptide fits the thickness of the membrane hydrophobic core, the peptide inserts into the membrane and adopts a TM orienta-

* This work was supported by Ministère de la Région Wallonne Contract 14540 (PROTMEM) and Contract 215140 (αBUSTEC). The costs of publication of this article were defrayed in part by the payment of page charges. This article must therefore be hereby marked "*advertisement*" in accordance with 18 U.S.C. Section 1734 solely to indicate this fact.

[1] These authors contributed equally to this work.
[2] Supported by National Fund for Scientific Research of Belgium Grant F.N.R.S.-Televie 7.4.527.05.F.
[3] Research Director at INSERM (France).
[4] Holder of the Harold S. and Harriet B. Brady Professorial Chair in Cancer Research. Supported by the Israel Science Foundation.
[5] Research Director of the National Funds for Scientific Research of Belgium. To whom correspondence should be addressed. Tel.: 32-81-62-25-21; Fax: 32-81-62-25-22; E-mail: brasseur.r@fsagx.ac.be.

[6] The abbreviations used are: TM, transmembrane; DOPC, 1,2-dioleoyl-*sn*-glycero-3-phosphocholine; DOPG, 1,2-dioleoyl-*sn*-glycero-3-phospho-racemic-(1-glycerol); DOPE, 1,2-dioleoyl-*sn*-glycero-3-phosphoethanolamine; CHOL, cholesterol; SM, sphingomyelin; LUV, large unilamellar vesicle; SUV, small unilamellar vesicle; FTIR, Fourier transform infrared; ATR, attenuated total reflection; TFE, trifluoroethanol; DPX, *N*,*N*′-*p*-xylenebis (pyridinium bromide); HPTS, 8-hydroxypyrene-1,3,6-trisulfonic acid; IMPALA, integral membrane protein and lipid association.

tion (26, 33). When it does not fit, either polar residues are exposed to the apolar medium, or hydrophobic residues are accessible to the water phase. This unfavorable phenomenon has been called hydrophobic mismatch (6, 16, 18, 34). Positive and negative hydrophobic mismatches occur when the hydrophobic stretch of a peptide is too long or too short with respect to the membrane thickness, respectively (16). The peptide can adapt its structure or its orientation to overcome mismatch (23, 25, 35). It can also oligomerize to reduce the mismatch (for a review, see Ref. 16). If the mismatch is too great, insertion of the peptide into the membrane is reduced (16, 34–37). It has been shown that membrane adaptation can also result as a response to a hydrophobic mismatch. ^{2}H NMR measurements with lipids containing a perdeuterated acyl chain, x-ray diffraction, and differential scanning calorimetry measurements revealed that a positive mismatch increases the lipid chain order, whereas a negative mismatch increases membrane disorder (38–41). However, other studies using ^{15}N as well as ^{31}P NMR, differential scanning calorimetry, and ESR showed that peptides long enough or too long to span the membrane perturb the membrane order whereas peptides that are too short have less effect (23, 24).

Few studies have focused on the ability of TM model peptides to induce membrane fusion. Hofmann *et al.* (42) showed that the fusogenicity of TM model peptides varies with the ratio of helix-promoting leucine and sheet-promoting valine residues and is enhanced if helix-destabilizing residues, such as glycine and proline, are present within their hydrophobic core. They further showed that fusogenicity of these peptides correlates with structural flexibility (42). The more flexible the peptide is, the more fusion is induced.

In this study, we analyzed the interaction of *de novo* TM peptides with membranes and in particular their ability to induce fusion. We designed three TM model peptides; all have a hydrophobic core made of alanines and leucines (14, 18, and 22 residues), and both the N and C termini were extended with three positively charged residues. Interactions and fusogenic properties of each KALR with a membrane were studied by modeling and experimental approaches.

EXPERIMENTAL PROCEDURES

Materials—1,2-Dioleoyl-*sn*-glycero-3-phosphocholine (DOPC), 1,2-dioleoyl-*sn*-glycero-3-phospho-racemic-(1-glycerol) sodium salt (DOPG), 1,2-dioleoyl-*sn*-glycero-3-phosphoethanolamine (DOPE), cholesterol (CHOL), and bovine brain sphingomyelin (SM) were purchased from Sigma. Trifluoroethanol (TFE), Hepes, Triton X-100, and Me_2SO were purchased from Sigma. Octadecylrhodamine chloride B, *N,N′-p*-xylenebis(pyridinium bromide) (DPX), and 8-hydroxypyrene-1,3,6-trisulfonic acid (HPTS) came from Molecular Probes, Inc. (Eugene, OR). NaCl came from Merck Eurolab (Leuven, Belgium). Peptides $KALR_{14}$, $KALR_{18}$, and $KALR_{22}$ were synthesized by NeoMPS (Strasbourg, France). These peptides have free N and C termini (Table 1). Their purity is higher than 85%.

Liposome Preparation—DOPC, DOPG, DOPE, SM, and CHOL were dissolved in a chloroform/methanol (2:1, v/v) solution. DOPC/CHOL/DOPE/DOPG/SM (34:33:16:10:7 mol/mol/mol/mol/mol) film was obtained after evaporation under vacuum with a rotary evaporator (Rotovapor R-3000, Van Der Heyden Büchi, Switzerland). The lipid film, dried for one night, was then dispersed in 2 ml of 5 mM HEPES and 100 mM NaCl, pH 7.4, buffer and incubated for 1 h at 37 °C. To obtain DOPC/CHOL/DOPE/DOPG/SM (34:33:16:10:7, mol/mol/mol/mol/mol) large unilamellar vesicles (LUV), the hydrated lipid dispersion was exposed to five freeze-thaw cycles and passed 10 times through a polycarbonate membrane (0.1 μm) under 20 bars pressure with an extruder (Lipex Biomembranes, Vancouver, Canada). To obtain DOPC/CHOL/DOPE/DOPG/SM (34/33/16/10/7 mol/mol/mol/mol/mol) small unilamellar vesicles (SUV), the hydrated film was sonicated (high intensity ultrasonic processor; Sigma) for 5 min at 50 W. A 10,000 $\times$ *g* centrifugation for 2 min (Biofuge Pico, Van der Heyden, Heraeus, Germany) discarded titanium deposit and residual multilamellar vesicles. The phospholipid concentration was determined by phosphorus analysis (43).

Lipid-binding Experiments—In a polar environment, the tryptophan present in KALRs has a fluorescence spectrum with a maximum around 350 nm. Upon the addition of SUVs, the fluorescence maximum shifts to the blue, around 335 nm. The affinity of the peptide for the SUV was determined by adding increasing amounts of vesicles to 0.67 mM peptides dissolved in Me_2SO, as previously described (44–46). Fluorescence was recorded at room temperature (λ_{exc}, 280 nm; λ_{em}, 335 nm) after each addition on an LS-50B PerkinElmer Life Sciences fluorimeter. The fluorescence values were then corrected by taking into account the dilution factor corresponding to the addition of the liposomes and by subtracting the corresponding blank (Me_2SO with the same amount of SUVs). The ratio (R) of bound to total peptides and the dissociation constant (K_d) were calculated as described by Lear and DeGrado (46). Experiments were carried out in a buffer composed of 5 mM HEPES and 100 mM NaCl at pH 7.4.

Lipid Mixing Experiments—Mixing of liposome membranes was followed by measuring the fluorescence increase of octadecylrhodamine chloride B, a lipid soluble probe, after the fusion of labeled and unlabeled liposomes. Labeled liposomes were obtained by incorporating octadecylrhodamine chloride B in the dry lipid film at a 5% concentration of the total lipid weight. Labeled and unlabeled liposomes were mixed at a weight ratio of 1:4, respectively, and at a final concentration of 12.5 μM in 5 mM HEPES and 100 mM of NaCl buffer at pH 7.4. 100% of fusion was determined by adding Triton X-100 at 2% to labeled/unlabeled (1:4) LUVs. Fluorescence was recorded at room temperature (λ_{exc}, 560 nm; λ_{em}, 590 nm) on an LS-50B PerkinElmer Life Sciences fluorimeter. The tests were performed with LUVs and were repeated three times with different batches of peptide.

Leakage of Liposome Vesicle Contents—Vesicle leakage was monitored using an assay based on the quenching of HPTS by DPX (47). HPTS and DPX are both encapsulated in the aqueous phase of the same liposomes. Leakage of vesicles was followed by measuring the dequenching of HPTS released into the medium. Fluorescence was recorded at room temperature (λ_{exc}, 450 nm; λ_{em}, 512 nm) on an LS-50B PerkinElmer fluorimeter. Liposomes (LUVs) were prepared as described above in 12.5 mM HPTS (45 mM NaCl), 45 mM DPX (20 mM NaCl), and 10 mM HEPES buffer at pH 7.4. Vesicles containing encapsu-

lated HPTS and DPX were eluted in the void volume of a Sephadex G-75 column, with 5 mM HEPES and 100 mM NaCl buffer (pH 7.4). Assays were repeated three times with different batches of peptide.

Electron Microscopy—The effect of the peptides on SUV was examined by negative transmission staining electron microscopy. Prior to staining and fixing, suspensions of SUV at 4.5 mM (with or without lyophilized peptide) were incubated for 5 min at room temperature. A drop containing SUV alone or with a peptide was deposited onto a carbon-coated grid and negatively stained with 2% phosphotungstic acid (pH 6.8). The grids were observed by using a JEOL JEM 100B electron microscope (Japan Electron Optics Laboratory Co., Tokyo, Japan).

IR Spectroscopy Measurements—Spectra were recorded at room temperature on a Brüker Equinox 55 equipped with a liquid nitrogen-cooled mercury-cadmium-telluride detector at a resolution of 2 cm^{-1} by averaging 512 scans. Reference spectra of the germanium plate were automatically recorded after purging for 15 min with dry air and subtracted from the recently run sample spectrum. The plate was sealed in a universal sample holder and rehydrated by flushing the holder with N_2 saturated with D_2O for 3 h at room temperature. Free peptide samples (50 μg of peptide in TFE) and the lipid-bound peptides were spread out on a germanium ATR plate (50 × 20 × 2 mm; Aldrich Chimica) with an aperture of 45°, yielding 25 internal reflections. The lipid-membrane sample was prepared by incubation of 1 ml of peptides at 60 μM with 6 ml of CHOL/DOPC/DOPE/DOPG (40/34/16/10, mol/mol/mol/mol/mol) SUV at 500 μM (1:50 peptide/lipid (mol/mol) ratio) in 5 mM HEPES and 100 mM NaCl buffer at pH 7.4 for 1 h at room temperature. After incubation, the lipid/peptide mixture was filtered through an anisotropic hydrophilic YM 30 membrane (cut-off 30 kDa) of a Centrifree micropartition system (Amicon) with a 13,000 × *g* centrifugation for 45 min to separate lipid-associated from free peptides. Distilled water was used to recuperate the retained sample containing the peptide-lipid complex. To determine the peptide insertion rate in membranes by infrared spectra, the area of the amide I peak was divided by the area of the lipid C=O peak and the number of amide groups in the peptide, as previously shown (35).

To evaluate the orientation of peptides in lipids, spectra were recorded at two orthogonal linear polarizations (90 and 0°) of the incident light. The dichroic spectrum was obtained by subtracting the spectrum recorded with polarized light at 0° from that at 90°. The angle between the germanium crystal and the dipole was calculated from the dichroic ratio $R_{ATR}/R_{ATR} = A(90°)/A(0°)$, where $A(90°)$ is the absorbance of the selected dipole from a spectrum recorded with polarized light at 90°, and $A(0°)$ is the absorbance of the same dipole from a 0° polarized spectrum. The bands chosen to characterize the protein and phospholipid orientation are the amide I and the lipid νs (CH_2), respectively (48, 49).

Design of KALRs—Three peptides with a hydrophobic core of 14, 18, and 22 residues were designed (Table 1). The hydrophobic core is an $AA(LAAA)_n$ motif with $n = 3$, 4, and 5 for $KALR_{14}$, $KALR_{18}$, and $KALR_{22}$, respectively. The hydrophobic core lengths were chosen to have variations of approximately one helix turn, corresponding to 6 Å (50). Each peptide is surrounded by three lysine residues at the N-terminal extremity and three arginine residues at the C-terminal extremity. At the center of the sequence of each peptide, a tryptophan residue replaces an alanine residue in order to have a fluorescent sensor.

Analysis by Molecular Modeling—The integral membrane protein and lipid association (IMPALA) method was used to analyze interaction of KALRs with membranes (51). The thickness of the implicit bilayer was extrapolated from experimental data on DOPC bilayers (16, 52, 53) and the contribution of SM/cholesterol to membrane thickness (54–57). The thickness of the model membrane was 40 Å with a hydrophobic core of 31 Å to mimic membranes used in the experimental assays.

The IMPALA method simulates the insertion of peptides into the bilayer by adding energy restraint functions to the usual energy function of peptides. The lipid bilayer is defined by $C(z)$, which represents an empirical function describing membrane properties as follows,

$$C(z) = 1 - \frac{1}{1 + e^{\alpha(z - z0)}} \qquad \text{(Eq. 1)}$$

where z is perpendicular to the membrane and has its origin at the center of the bilayer. The values α and $z0$ are parameters fixed in such a way that $C(|z \geq 20\ Å|) = 1$ and $C(|z \leq 15.5\ Å|) = 0$. The value of the function is constant from $-\infty$ to -20 Å (hydrophilic phase), from -15.5 to 15.5 Å (hydrophobic core), and from 20 Å to ∞ (hydrophilic phase).

Two restraints simulate the interaction between the peptide and the bilayer. The first one accounts for the effect that pushes hydrophobic atoms into the membrane (hydrophobic restraint) and hydrophilic atoms outside of it as follows,

$$E_{pho} = -\sum_{i=1}^{N} S(i)\,Etr(i)\,C(zi) \qquad \text{(Eq. 2)}$$

where N is the total number of atoms, $S(i)$ is the solvent-accessible surface of atom i, $Etr(i)$ is its transfer energy in units of accessible surface area, and $C(zi)$ is the value of $C(z)$ at the position zi of atom i.

The second restraint simulates the perturbation of the bilayer due to the insertion of the molecule (E_{lip}),

$$E_{lip} = a_{lip} \sum_{i=1}^{N} S(i)(1 - C(zi)) \qquad \text{(Eq. 3)}$$

where a_{lip} is an empirical factor fixed to 0.018 (51).

Peptides were constructed as α-helices using Hyperchem 6.0 (Hypercube, Inc.) assigning values of ϕ and ψ angles of -58 and -47°, respectively (50). Conformation of backbone and side chains was optimized with Hyperchem by a conjugated gradient procedure using the AMBER 3 force field with termination conditions fixed to a root mean square gradient of 0.01 k_{cal}/(Å·mol). A systematic procedure was performed to predict the position of the peptide into the membrane. During this procedure, the peptide systematically moves from 40 to -40 Å with

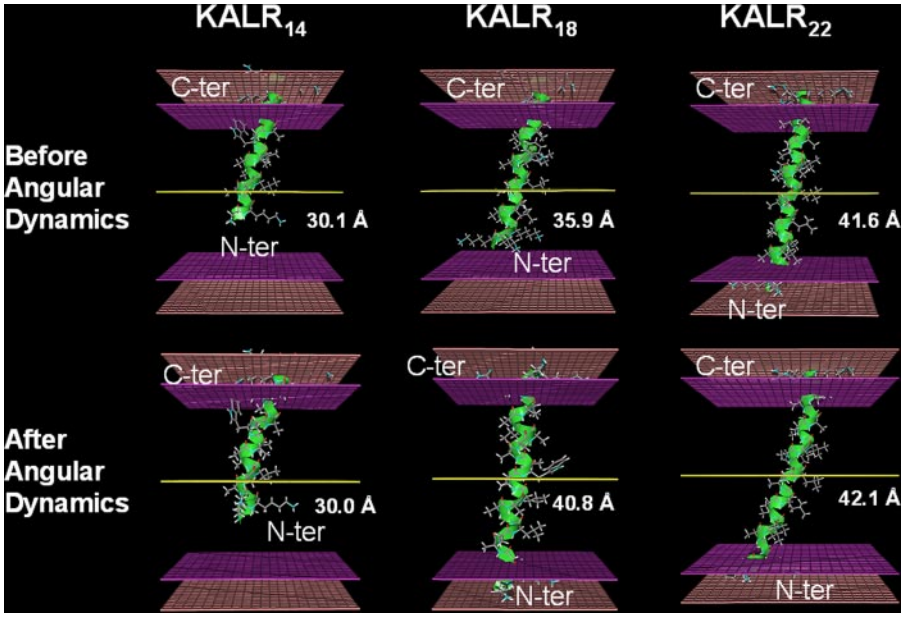

FIGURE 1. **Best positions of KALRs in membrane as predicted by IMPALA before and after angular dynamics.** For each peptide, N and C termini and lengths of the backbone are indicated. *Yellow plane*, bilayer center (z = 0); *purple planes*, lipid acyl chain/polar head group interfaces at 15.5 Å from the center; *pink planes*, lipid/water interfaces at 20 Å from the center.

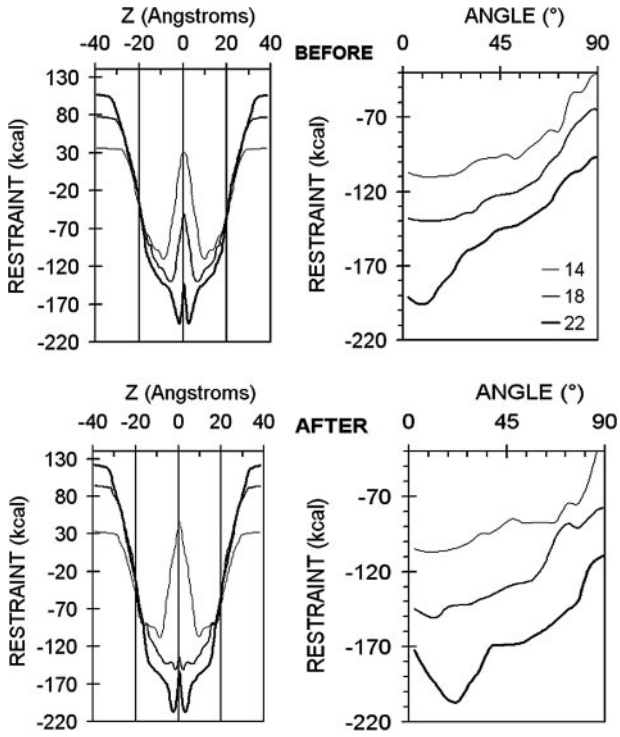

FIGURE 2. **IMPALA restraints as a function of the peptide mass center penetration (*left*) and the peptide helix-axis angle (*right*) before and after angular dynamics.** The helix-axis angle is calculated with respect to the normal to the membrane, and the mass center penetration is measured with respect to the membrane center. *14*, $KALR_{14}$; *18*, $KALR_{18}$; *22*, $KALR_{22}$.

respect to the membrane center in steps of 1 Å. For each position along the z axis, 5000 random orientations are tested. At the end of the systematic analysis, the position and the orientation with minimal energy among the 405,000 positions tested are selected. The peptide structure was optimized by an angular dynamics procedure taking into account the force field of the membrane as described by Lins *et al.* (58). Random rotations of 2° maximum and random translations of 0.1 Å maximum of the peptide are allowed. Calculations were performed on an Intel® Pentium® 4, CPU 3.80 GHz, 4.00 gigabytes of RAM. Graphs were drawn using WinMGM (59).

RESULTS

Study of KALRs in an Implicit Membrane Model—The IMPALA algorithm, which successfully predicted the interaction of many peptides with membranes (7, 8, 51, 60), was used to predict the interaction of the KALRs with a model membrane mimicking plasma membranes (Fig. 1). Each KALR was folded as a standard helix, and its interaction at all levels of the membrane was analyzed by a systematic procedure. Then peptide was set at its best level of insertion and was left to adapt in the membrane by an angular dynamics procedure.

After angular dynamics, the three peptides remain mainly helical, although some structure adaptations occur to minimize the sum of intramolecular energy plus the IMPALA restraints (data not shown). The root mean square deviation values between the peptide backbone before and after angular dynamics are 1.1, 1.3, and 0.9 Å for $KALR_{22}$, $KALR_{18}$, and $KALR_{14}$, respectively. Structural changes of $KALR_{22}$ have a minor effect on the length of the peptide (elongation of 0.5 Å). $KALR_{18}$ length increases from 35.9 to 40.8 Å due to the transition from α-helix to more extended structures, especially at the N- and C-terminal extremities. Like $KALR_{22}$, $KALR_{14}$ undergoes relatively low backbone deformation and no elongation of structure (variation of 0.1 Å).

$KALR_{22}$, $KALR_{18}$, and $KALR_{14}$ angles, with respect to the membrane normal, are 10, 15, and 15° before angular dynamics, and 20, 10, and 10° afterward (Figs. 1 and 2). Thus, the three KALRs adopt a perpendicular orientation. However, the transmembranous status depends on the peptide. $KALR_{22}$ spans the entire membrane, similarly folded before and after structure optimization. Its mass center is 2 Å away from the membrane center (Figs. 1 and 2). Its polar extremities are outside the hydrophobic core of the membrane, and its hydrophobic core is inside. Before the angular dynamics, $KALR_{18}$ does not traverse the membrane and has its charged N-terminal extremity in the hydrophobic core of the membrane (Fig. 1). Its mass center is 6 Å away from the membrane center (Fig. 2). After the angular dynamics, it traverses the membrane due to peptide elongation. Its two polar extremities are located outside the hydrophobic core of the membrane (Fig. 1), and its mass center is closer to the membrane center (1 Å). Compared with $KALR_{18}$, the position of $KALR_{14}$ in the membrane does not

change after the angular dynamics. The peptide mass center is at 10 Å away from the membrane center (Fig. 2). In this position, the N-terminal extremity is exposed to the hydrophobic core of the membrane (Fig. 1). Hence, if all peptides are perpendicular to the membrane and two cross that membrane, one is restricted to one monolayer.

The energy profiles of $KALR_{22}$ in the membrane are similar before and after angular dynamics (Fig. 2). The peptide is well inserted into the membrane and does not need structural optimization to locate hydrophobic residues in the membrane core and hydrophilic residues at the interface. The energy profiles also show that the TM position is much more energetically favorable than non-TM positions. The energy profiles of $KALR_{18}$ are different before and after angular dynamics (Fig. 2). After optimization, the interaction of $KALR_{18}$ with the membrane is energetically more favorable than before, especially for TM positions with the mass centers of the peptide around the center of the membrane ($Z = 0$ Å). This is due to elongation of the peptide backbone and the consequent migration of the polar N-terminal extremity from the apolar membrane core to polar lipid head groups. The energy profiles of $KALR_{14}$ in the membrane are similar before and after angular dynamics (Fig. 2). Since the peptide can only traverse one monolayer, the interaction energy is much less favorable than for longer peptides, and interfacial positions are more stable than positions at the center of the membrane. The ability of $KALR_{14}$ to adopt nonperpendicular positions is greater than for the other peptides.

Binding of KALRs to Membranes—The affinity of the three peptides for DOPC/CHOL/DOPE/DOPG/SM (34/33/16/10/7, mol/mol/mol/mol/mol) SUVs was monitored by following the fluorescence of the central tryptophan residue (Table 1). When the peptide interacts with lipids, the tryptophan emission wavelength shifts from 350 to 335 nm (Fig. 3*A*). The binding of KALRs to membranes was measured at 335 nm upon titration with SUVs. An increase in the fluorescence intensity corresponds to an increase in the amount of membrane-bound peptides. For the three peptides, fluorescence increases when SUVs are added (Fig. 3*B*). All three peptides bind strongly to membranes, although with different affinities. The partition coefficients calculated from the curves are 7×10^5, 2×10^6, and 4.5×10^6 for $KALR_{14}$, $KALR_{18}$, and $KALR_{22}$,respectively. The data reveal a direct correlation between the peptide length and its binding capability; an increase in the peptide length by 4 residues results in about a 2.5-fold higher partition coefficient.

Structural Properties of KALRs—Fourier transform infrared (FTIR) spectroscopy was used to determine the structure of each KALR in TFE solvent and within membranes (Fig. 4, *A* and *B*). The spectral position of the amide I vibration, between 1615.5 and 1694.5 cm^{-1}, was used to characterize the conformation of the peptide backbone (48). No significant difference was observed between the three peptides in the different media (Fig. 4). Indeed, the bands are centered around 1655 cm^{-1}, indicating that they are mainly helical in TFE as well as in phospholipids (Figs. 4, *A* and *B*).

As shown in Fig. 4*B*, the intensity of the amide I absorption band is sensitive to the length of the peptide when inserted into lipids. A decrease in the band intensity is observed when the length of the peptide decreases, with a considerable decrease for the shortest peptide. Since the buffer gives no significant FTIR signal (data not shown), these data indicate that the longest peptide is the most inserted into the bilayer. From the FTIR spectra, we evaluated the relative insertion of each peptide into membranes (35). If we consider that the $KALR_{22}$ peptide has an insertion rate of 100, $KALR_{18}$ and $KALR_{14}$ have a relative rate of 90 and 40, respectively. In summary, the FTIR analysis reveals that KALR inserts into membranes as an α-helix conformation and that the amount of inserted peptides depends on its length.

Orientation of KALRs in the Bilayer—The orientation of peptides in lipid bilayers was calculated by recording the spectra obtained with polarized IR lights parallel and perpendicular with respect to the incidence plane. The amide I transition moment, around 1655 cm^{-1}, is parallel to the helix axis, whereas

TABLE 1
Sequence of KALR peptides
Shown are the sequences of KALR peptides. N and C termini of the peptides are free.

Peptide	Sequence
$KALR_{14}$	KKKAALAAALWAALAAARRR
$KALR_{18}$	KKKAALAAALAAWLAAALAAARRR
$KALR_{22}$	KKKAALAAALAAALWAALAAALAAARRR

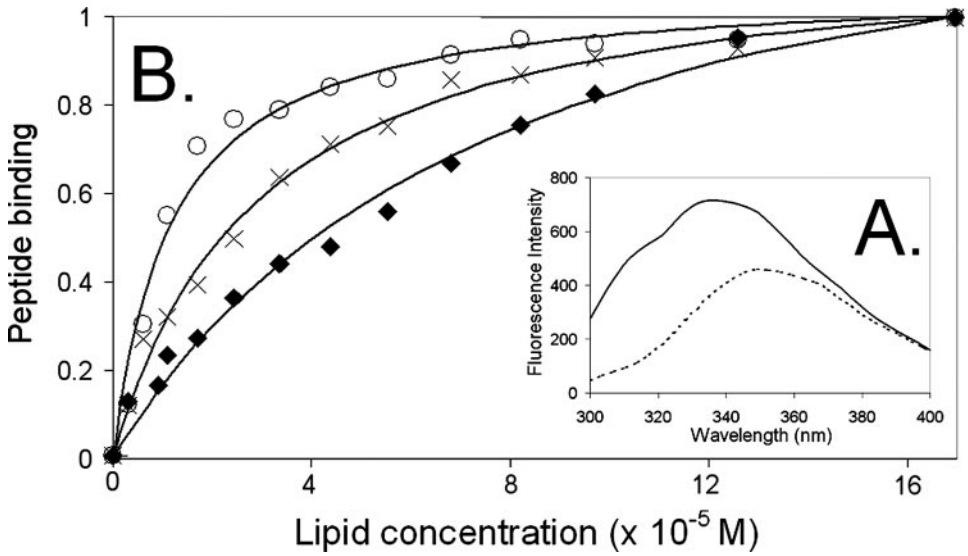

FIGURE 3. *A*, emission spectra of the $KALR_{22}$ peptide alone (*dotted line*) and in the presence of DOPC/CHOL/DOPE/DOPG/SM (34/33/16/10/7 m/m) SUVs (*full line*). The excitation wavelength was set at 280 nm (8-nm slit). *B*, membrane binding affinity of KALR peptides. Increase in peptide fluorescence upon titration with DOPC/CHOL/DOPE/DOPG/SM (34/33/16/10/7, mol/mol/mol/mol/mol) SUVs. The excitation wavelength was set at 280 nm (8-nm slit), and the excitation was recorded at 335 nm (8-nm slit). ♦, $KALR_{14}$ peptide; ×, $KALR_{18}$ peptide; ○, $KALR_{22}$ peptide.

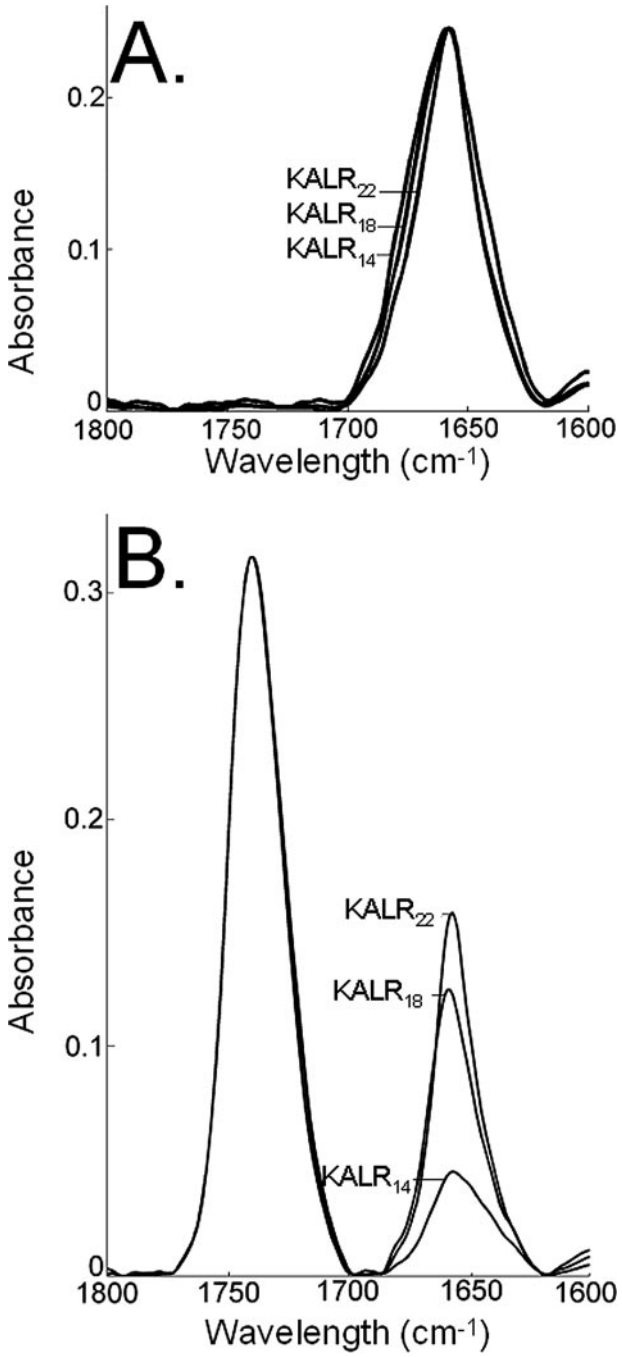

FIGURE 4. **Infrared spectra of KALRs in TFE and in membranes.** Infrared spectra of $KALR_{14}$, $KALR_{18}$, and $KALR_{22}$ in TFE (*A*) or inserted in CHOL/DOPC/DOPE/DOPG (40/34/16/10, mol/mol/mol/mol) LUVs (*B*).

the transition moment for $\nu s(CH_2)$, around 2853 cm^{-1}, is perpendicular to the lipid chain axis. These bands were used to evaluate the orientation of the peptide helix axis and the lipid chain axis with respect to the germanium plate by calculating their dichroic ratios (48, 49). The R_{ATR} of the lipid $\nu s(CH_2)$ is 1.43 for all peptides. This corresponds to an angle of 41 ± 5° between the acyl chain carbons and the normal to the germanium crystal (Table 2). This value is comparable with that obtained by Castano and Desbats with similar membranes (49). The R_{ATR} of the amide I band yields a helix axis angle of 53, 46, and 43 ± 5° compared with the germanium plate normal for

TABLE 2

Dichroic ratio and angle of the KALRs and phospholipid acyl chains with respect to the germanium plate

Shown are the dichroic ratio (R_{ATR}) and angle of the KALR α-helices and of phospholipid acyl chains with respect to the normal to the germanium plate.

Peptide	α-Helix		Phospholipids		α-Helix/phospholipid angle[a]
	R_{ATR}	Angle	R_{ATR}	Angle	
		degrees		*degrees*	*degrees*
$KALR_{14}$	1.61	53 ± 5	1.43	41 ± 5	12 ± 10
$KALR_{18}$	1.71	46 ± 5	1.43	41 ± 5	5 ± 10
$KALR_{22}$	1.75	43 ± 5	1.43	41 ± 5	2 ± 10

[a] Relative angle between the KALR α-helices and the phospholipid acyl chains.

$KALR_{14}$, $KALR_{18}$, and $KALR_{22}$, respectively. From these data, we can calculate that helix axes of $KALR_{14}$, $KALR_{18}$, and $KALR_{22}$ adopt a mean angle with respect to the membrane normal equal to 12, 5, and 2 ± 10°, respectively (Table 2). ATR-FTIR spectra thus indicate that KALRs are perpendicular helices in membranes.

Studying the Fusogenic Properties of KALRs—We first studied the fusogenic capacity of peptides by measuring their ability to induce lipid mixing of liposomes (Fig. 5, *A* and *B*). $KALR_{14}$ induces no significant liposome lipid mixing, even after 10 min of incubation. The longer peptides, $KALR_{18}$ and $KALR_{22}$, induce lipid mixing of liposomes. The lipid mixing increases rapidly following the addition of $KALR_{22}$ and reaches a maximum after only 60 s. For $KALR_{18}$, the maximum is reached after 240 s. Analysis of lipid mixing at different peptide/lipid ratios confirmed that the smallest peptide has no significant effect as compared with the longer peptides and that $KALR_{22}$ induces more lipid mixing than $KALR_{18}$ irrespective of the peptide/lipid ratio (Fig. 5*B*). The lipid mixing induced by $KALR_{22}$ and $KALR_{18}$ increases with the peptide/lipid ratio and is maximal at a ratio of 0.04. Above this ratio, lipid mixing decreases. $KALR_{22}$ induces a maximal lipid mixing of about 50% of the liposomes.

To further investigate the membrane-destabilizing effect of KALRs, we carried out leakage assays. The addition of $KALR_{14}$ to membrane liposomes does not increase leakage, whereas the addition of $KALR_{18}$ or $KALR_{22}$ does (Fig. 5*C*). Similar to the lipid mixing assays, the process is dose-dependent with a maximum response for a peptide/lipid ratio of 0.04. Above this ratio, leakage decreases. $KALR_{22}$ also induces more leakage than $KALR_{18}$ irrespective of the peptide/lipid ratio and the incubation time (Fig. 5, *C* and *D*). $KALR_{22}$ induces a maximal leakage of about 80% of the liposomes.

To analyze the effect of KALRs on membranes, we observed LUVs by negative stain electron microscopy before and after the addition of peptides (peptide/lipid ratio = 0.04). Micrographs show that $KALR_{14}$ has no effect on LUVs (Fig. 6). The increase in vesicle size in the presence of $KALR_{18}$ demonstrates fusion. $KALR_{22}$ also increases vesicle size but to a larger extent.

DISCUSSION

In this paper, we examined the ability of hydrophobic TM model peptides with three hydrophobic core lengths to induce *in vitro* membrane fusion and its correlation with membrane binding, membrane insertion, and the ability to induce membrane destabilization. These peptides, called KALRs, are composed of hydrophobic residues (Ala and Leu residues) sur-

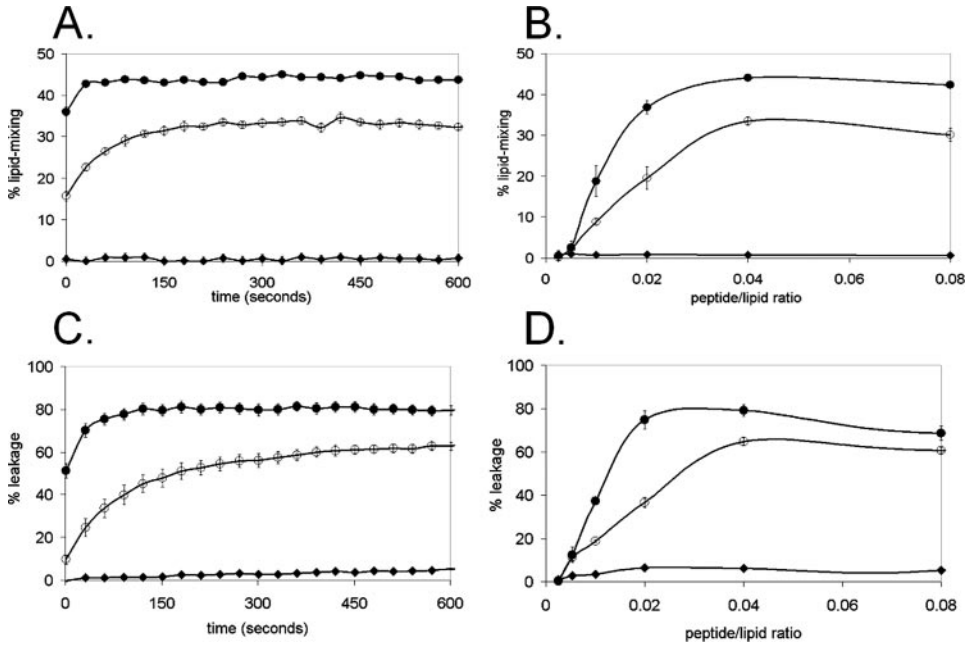

FIGURE 5. **Liposome lipid mixing and leakage induced by KALRs.** *A*, lipid mixing of DOPC/CHOL/DOPE/DOPG/SM (34/33/16/10/7 mol/mol/mol/mol/mol) LUVs induced by KALRs as a function of time at a peptide/lipid ratio of 0.04. *B*, lipid mixing induced by KALRs as a function of the peptide/lipid ratio. *C*, time course of leakage of DOPC/CHOL/DOPE/DOPG/SM (34/33/16/10/7, mol/mol/mol/mol/mol) LUVs induced by KALRs at a peptide/lipid ratio of 0.04. *D*, leakage induced by KALRs as a function of the peptide/lipid ratio. ♦, $KALR_{14}$; ○, $KALR_{18}$; ●, $KALR_{22}$.

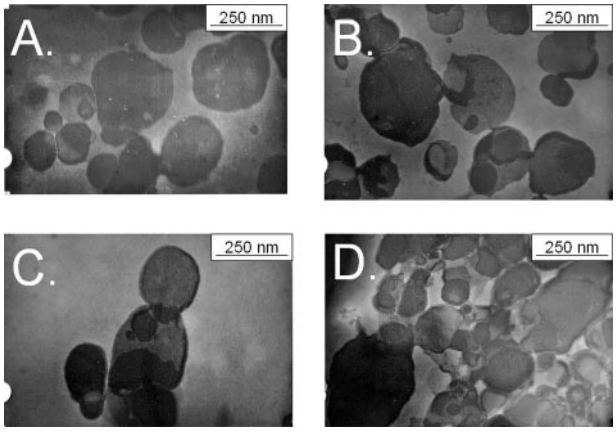

FIGURE 6. **Electron microscopy images of negatively stained DOPC/CHOL/DOPE/DOPG/SM (34/33/16/10/7, mol/mol/mol/mol/mol) LUVs.** *A*, in the absence of peptide. *B*, in the presence of $KALR_{14}$. *C*, in the presence of $KALR_{18}$. *D*, in the presence of $KALR_{22}$.

rounded by charged residues (Lys and Arg residues). The hydrophobic part is a repeat of 3, 4, and 5 AAAL motifs that result in a difference of approximately one turn of helix between peptides.

Effect of the Hydrophobic Core Length of KALR on Insertion into Membranes—Lipid-binding assays and infrared spectroscopy show that the ability of KALRs to bind to lipids and to be incorporated into membranes increases with the length of the hydrophobic core of the peptides. These results could simply be explained by the hydrophobicity of peptides. Indeed, the addition of one AAAL motif increases the peptide and the helix structure's hydrophobicity (as seen in Fig. 2), and as a result, affinity for lipids is multiplied by 2.5, as measured in the lipid-binding assays. However, the insertion rate of KALRs into membranes calculated from FTIR spectra is not linearly related to the addition of AAAL motifs. Indeed, the insertion rate of $KALR_{14}$ is 40% that of $KALR_{22}$, whereas the insertion rate of $KALR_{18}$ is 90%. This indicates that insertion of KALR peptides into lipids is not simply governed by hydrophobicity.

The hydrocarbon thickness of a fully hydrated DOPC bilayer is 26.8–28.6 Å (16, 52, 53, 61–63). The addition of SM and cholesterol increases the thickness of the hydrophobic core of monounsaturated membranes by 2–4.1 Å (54–57). It was also shown that in some cases, SM and cholesterol can induce the formation of more rigid lipidic domains 3–10 Å thicker than the rest of the membrane (56, 64, 65). We can conclude from these data that at least a large part of our DOPC membrane has a hydrophobic thickness between 28.8 and 32.7 Å. Thicker rigid domains could be present, but this cannot be assumed with certainty. That is why the membrane hydrophobic core is 31 Å thick in the molecular modeling simulation.

The first result of molecular modeling simulations is that all KALR helical peptides adopt a perpendicular orientation in membranes. This prediction is in accordance with the FTIR data of this study and with previous studies showing that Ala/Leu peptides of different lengths are transmembrane helices in membranes (11, 16, 17, 30, 35).

The second result of molecular modeling simulations is that the compatibility between membranes and peptides depends on the peptide length. $KALR_{22}$ matches the membrane thickness; it inserts the hydrophobic residues inside the membrane hydrophobic core and allows the hydrophilic residues to protrude from the membrane. In contrast, $KALR_{14}$ is too short to traverse the membrane even with structural adaptations; the N terminus is located in the membrane core, which is energetically unfavorable. This situation corresponds to a negative hydrophobic mismatch. In between, $KALR_{18}$ is too short to span the membrane as a standard α-helix, but structural optimization elongates the helix and suppresses this incompatibility. These results are consistent with previous studies of peptide-membrane hydrophobic mismatch. Small distortions of α-helix structure can occur at the extremities of a TM model peptide too short to span a membrane (16, 66). To reduce the mismatch, other adaptations, such as peptide oligomerization or lipid length reduction, can occur (for a review, see Ref. 16). However, when the mismatch is too great, the peptide is excluded from the membrane (23, 34). This would explain why the $KALR_{14}$ is much less inserted into the membrane than $KALR_{18}$ and $KALR_{22}$.

In conclusion, peptide-membrane interactions depend on peptide hydrophobicity and on the matching of peptide length with membrane thickness. Peptide hydrophobicity should mainly control its ability to bind to lipids. In addition, the peptide's length should affect the peptide's ability to insert into a membrane. $KALR_{18}$ should have reduced binding and insertion with respect to $KALR_{22}$ because of a lower hydrophobicity and of a small hydrophobic mismatch. The lower hydrophobicity and the large hydrophobic mismatch of $KALR_{14}$ should decrease its insertion into membranes.

Furthermore, this work serves as another piece of evidence that IMPALA can be used to predict how a peptide will interact with a membrane. IMPALA can predict the insertion and orientation, the impact on the peptide structure, and the degree of hydrophobic mismatch.

Effect of the Hydrophobic Core Length of KALR on Fusogenicity—Previous studies showed that peptides corresponding to the TM domain of the vesicular stomatitis virus G protein and of SNARE induce *in vitro* membrane fusion (67–69). It was proposed that the fusogenicity of TM domains depends on structural flexibility (67–69). The relationship between TM peptide fusogenicity and structural flexibility was further shown by using a TM model peptide with variable proportions of α-helix/β-sheet-promoting residues (42). Here we showed that a TM model peptide can induce membrane fusion *in vitro* even if it contains only alanine and leucine α-helix-promoting residues (70–72) as long as the length of the hydrophobic core is sufficient.

Differential scanning calorimetry, NMR, x-ray, and ESR studies already revealed that the length of TM model peptides has an effect on their ability to destabilize membranes (14, 23, 24, 28, 39, 40, 73–80). In general, destabilization is observed when the peptide is too short to span the membrane (14, 28, 39, 40, 74, 75). The extent of destabilization is related to the extent of negative hydrophobic mismatch (14, 28, 39, 74, 75). Conversely, membrane destabilization was also reported for TM model peptides that match the membrane or that are slightly too long (23, 24, 28, 76, 78–80). In some cases, the destabilizing effect decreases when the peptide length decreases (23, 24, 76).

Our study goes in the same direction as the latter studies; the longer the peptide, the more it induces fusion *in vitro*. This could first be related to the number of membrane-inserted peptides. Destabilization of a membrane can be greater if more peptides insert into it (23, 24). Membrane destabilization would then increase with KALR length, because the quantity of inserted peptides increases with length. However, $KALR_{14}$ does not induce membrane fusion whenever its insertion rate is 40% of the $KALR_{22}$ rate. Hence, fusogenicity must be controlled by additional parameters whose insertion rate is also supported by the fact that many TM peptides are not fusogenic.

Molecular modeling results suggest that one of the parameters regulating fusogenicity might be peptide length. Indeed, $KALR_{14}$ spans only one monolayer of the membrane, whereas $KALR_{18}$ and $KALR_{22}$ can traverse the bilayer. It was previously shown that hemagglutinin of the influenza A virus needs to have a TM domain of at least 17 residues to efficiently promote full fusion (81). When the TM domain has only 16 or fewer residues, the hemagglutinin cannot promote full fusion (81). Interestingly, the minimal length for fusogenicity is in the same range for different peptides: 17 residues for HA2 and between 14 and 18 residues for the KALR peptide. An effect of the length of the TM domain on the fusion process was also described previously for other viruses, such as human immunodeficiency virus (82), Foamy virus (83), murine coronavirus (84), and murine leukemia virus (85), and for SNARE protein (86, 87). The capacity to span the membrane might be an important parameter for inducing fusion.

Acknowledgments—We thank Prof. E. Goormaghtigh for advice on infrared spectroscopy and Dr. L. Lins for advice on molecular modeling.

REFERENCES

1. Hauser, H., and Poupart, G. (2005) in *The Structure of Biological Membranes*, 2nd Ed. (Yeagle, P. L., ed) CRC Press LLC, Boca Raton, FL
2. Eiler, S., Gangloff, M., Duclaud, S., Moras, D., and Ruff, M. (2001) *Protein Expression Purif.* **22,** 165–173
3. Nakayama, M., and Ohara, O. (2003) *Biochem. Biophys. Res. Commun.* **312,** 825–830
4. Martin, I., and Ruysschaert, J. M. (2000) *Biosci. Rep.* **20,** 483–500
5. Busquets, M. A., Alsina, M. A., and Haro, I. (2003) *Curr. Drug Targets* **4,** 633–642
6. Weiss, T. M., van der Wel, P. C. A., Killian, J. A., Koeppe, R. E., and Huang, H. W. (2003) *Biophys. J.* **84,** 379–385
7. Lorin, A., Thomas, A., Stroobant, V., Brasseur, R., and Lins, L. (2006) *Chem. Phys. Lipids* **141,** 185–196
8. Charloteaux, B., Lorin, A., Crowet, J. M., Stroobant, V., Lins, L., Thomas, A., and Brasseur, R. (2006) *J. Mol. Biol.* **359,** 597–609
9. Davis, J. H., Clare, D. M., Hodges, R. S., and Bloom, M. (1983) *Biochemistry* **22,** 5298–5305
10. Bechinger, B. (1996) *J. Mol. Biol.* **263,** 768–775
11. Bechinger, B. (2001) *Biophys. J.* **81,** 2251–2256
12. Zhao, J. B., Kimura, S., and Imanishi, Y. (1996) *Biochim. Biophys. Acta* **1283,** 37–44
13. Liu, L. P., Li, S. C., Goto, N. K., and Deber, C. M. (1996) *Biopolymers* **39,** 465–470
14. Killian, J. A., Salemink, I., de Planque, M. R. R., Lindblom, G., Koeppe, R. E., and Greathouse, D. V. (1996) *Biochemistry* **35,** 1037–1045
15. Lewis, R. N. A. H., Zhang, Y. P., Hodges, R. S., Subczynski, W. K., Kusumi, A., Flach, C. R., Mendelsohn, R., and McElhaney, R. N. (2001) *Biochemistry* **40,** 12103–12111
16. de Planque, M. R. R., and Killian, J. A. (2003) *Mol. Membr. Biol.* **20,** 271–284
17. Ozdirekcan, S., Rijkers, D. T. S., Liskamp, R. M. J., and Killian, J. A. (2005) *Biochemistry* **44,** 1004–1012
18. Killian, J. A. (2003) *FEBS Lett.* **555,** 134–138
19. Deber, C. M., Liu, L. P., Wang, C., Goto, N. K., and Reithmeier, R. A. F. (2002) *Curr. Top. Membr.* **52,** 465–479
20. Rinia, H. A., Boots, J.-W. P., Rijkers, D. T. S., Kik, R. A., Snel, M. M. E., Demel, R. A., Killian, J. A., Van der Eerden, J. P. J. M., and De Kruijff, B. (2002) *Biochemistry* **41,** 2814–2824
21. Chung, L. A., and Thompson, T. E. (1996) *Biochemistry* **35,** 11343–11354
22. Percot, A., Zhu, X. X., and Lafleur, M. (1999) *Biopolymers* **50,** 647–655
23. Harzer, U., and Bechinger, B. (2000) *Biochemistry* **39,** 13106–13114
24. Lewis, R. N. A. H., Zhang, Y. P., Liu, F., and McElhaney, R. N. (2002) *Bioelectrochemistry* **56,** 135–140
25. Sharpe, S., Barber, K. R., Grant, C. W. M., Goodyear, D., and Morrow, M. R. (2002) *Biophys. J.* **83,** 345–358
26. Strandberg, E., Ozdirekcan, S., Rijkers, D. T. S., van der Wel, P. C. A., Koeppe, R. E., Liskamp, R. M. J., and Killian, J. A. (2004) *Biophys. J.* **86,** 3709–3721
27. Sparr, E., Ash, W. L., Nazarov, P. V., Rijkers, D. T. S., Hemminga, M. A., Tieleman, D. P., and Killian, J. A. (2005) *J. Biol. Chem.* **280,** 39324–39331

28. Siegel, D. P., Cherezov, V., Greathouse, D. V., Koeppe II, R. V., Killian, J. A., and Caffrey, M. (2006) *Biophys. J.* **90,** 200–211
29. Killian, J. A., and Nyholm, T. K. M. (2006) *Curr. Opin. Struct. Biol.* **16,** 473–479
30. Zhang, Y. P., Lewis, R. N. A. H., Henry, G. D., Sykes, B. D., Hodges, R. S., and McElhaney, R. N. (1995) *Biochemistry* **34,** 2348–2361
31. Reithmeier, R. A. F. (1995) *Curr. Opin. Struct. Biol.* **5,** 491–500
32. Vonheijne, G. (1994) *Annu. Rev. Biophys. Biomol. Struct.* **23,** 167–192
33. de Planque, M. R. R., Boots, J. W. P., Rijkers, D. T. S., Liskamp, R. M. J., Greathouse, D. V., and Killian, J. A. (2002) *Biochemistry* **41,** 8396–8404
34. Ren, J. H., Lew, S., Wang, Z. W., and London, E. (1997) *Biochemistry* **36,** 10213–10220
35. de Planque, M. R. R., Goormaghtigh, E., Greathouse, D. V., Koeppe, R. E., Kruijtzer, J. A. W., Liskamp, R. M. J., de Kruijff, B., and Killian, J. A. (2001) *Biochemistry* **40,** 5000–5010
36. Moll, T. S., and Thompson, T. E. (1994) *Biochemistry* **33,** 15469–15482
37. Webb, R. J., East, J. M., Sharma, R. P., and Lee, A. G. (1998) *Biochemistry* **37,** 673–679
38. Zhang, Y. P., Lewis, R. N. A. H., Hodges, R. S., and McElhaney, R. N. (1992) *Biochemistry* **31,** 11579–11588
39. de Planque, M. R. R., Kruijtzer, J. A. W., Liskamp, R. M. J., Marsh, D., Greathouse, D. V., Koeppe, R. E., de Kruijff, B., and Killian, J. A. (1999) *J. Biol. Chem.* **274,** 20839–20846
40. Morein, S., Strandberg, E., Killian, J. A., Persson, S., Arvidson, G., Koeppe, R. E., and Lindblom, G. (1997) *Biophys. J.* **73,** 3078–3088
41. Morein, S., Killian, J. A., and Sperotto, M. M. (2002) *Biophys. J.* **82,** 1405–1417
42. Hofmann, M. W., Weise, K., Ollesch, J., Agrawal, P., Stalz, H., Stelzer, W., Hulsbergen, F., de Groot, H., Gerwert, K., Reed, J., and Langosch, D. (2004) *Proc. Natl. Acad. Sci. U. S. A.* **101,** 14776–14781
43. Mrsny, R. J., Volwerk, J. J., and Griffith, O. H. (1986) *Chem. Phys. Lipids* **39,** 185–191
44. Schwarz, G., Stankowski, S., and Rizzo, V. (1986) *Biochim. Biophys. Acta* **861,** 141–151
45. Rizzo, V., Stankowski, S., and Schwarz, G. (1987) *Biochemistry* **28,** 2751–2759
46. Lear, J. D., and DeGrado, W. F. (1987) *J. Biol. Chem.* **262,** 6500–6505
47. Van Bambeke, F., Kerkhofs, A., Schanck, A., Remacle, C., Sonveaux, E., Tulkens, P. M., and Mingeot-Leclerq, M. P. (2000) *Lipids* **35,** 213–223
48. Goormaghtigh, E., Raussens, V., and Ruysschaert, J. M. (1999) *Biochim. Biophys. Acta* **1422,** 105–185
49. Castano, S., and Desbat, B. (2005) *Biochim. Biophys. Acta* **1715,** 81–95
50. Creighton, T. E. (1992) *Proteins: Structures and Molecular Properties*, 2nd ed., pp. 182–186, W. H. Freeman and Co., New York
51. Ducarme, P., Rahman, M., and Brasseur, R. (1998) *Proteins* **30,** 357–371
52. Nagle, J. F., and Tristram-Nagle, S. (2000) *Biochim. Biophys. Acta* **1469,** 159–195
53. Kucerka, N., Tristram-Nagle, S., and Nagle, J. F. (2005) *J. Membr. Biol.* **208,** 193–202
54. Nezil, F. A., and Bloom, M. (1992) *Biophys. J.* **61,** 1176–1183
55. Cantor, R. S. (1999) *Biophys. J.* **76,** 2625–2639
56. Simons, K., and Vaz, W. L. C. (2004) *Annu. Rev. Biophys. Biomol. Struct.* **33,** 269–295
57. Salamon, Z., Devanathan, S., Alves, I. D., and Tollin, G. (2005) *J. Biol. Chem.* **280,** 11175–11184
58. Lins, L., Charloteaux, B., Heinen, A., Thomas, A., and Brasseur, R. (2006) *Biophys. J.* **90,** 470–479
59. Rahman, M., and Brasseur, R. (1994) *J. Mol. Graph.* **12,** 212–218
60. Lins, L., Charloteaux, B., Thomas, A., and Brasseur, R. (2001) *Proteins* **44,** 435–447
61. Lewis, B. A., and Engelman, D. M. (1983) *J. Mol. Biol.* **166,** 211–217
62. Tristram-Nagle, S., Petrache, H. I., and Nagle, J. F. (1998) *Biophys. J.* **75,** 917–925
63. Bystrom, T., Grobner, G., and Lindblom, G. (2003) *Colloids Surf.* **228,** 37–42
64. Milhiet, P. E., Domec, C., Giocondi, M. C., Van Mau, N., Heitz, F., and Le Grimellec, C. (2001) *Biophys. J.* **81,** 547–555
65. Saslowsky, D. E., Lawrence, J., Ren, X. Y., Brown, D. A., Henderson, R. M., and Edwardson, J. M. (2002) *J. Biol. Chem.* **277,** 26966–26970
66. Liu, F., Lewis, R. N. A. H., Hodges, R. S., and McElhaney, R. N. (2002) *Biochemistry* **41,** 9197–9207
67. Langosch, D., Crane, J. M., Brosig, B., Hellwig, A., Tamm, L. K., and Reed, J. (2001) *J. Mol. Biol.* **311,** 709–721
68. Langosch, D., Brosig, B., and Pipkorn, R. (2001) *J. Biol. Chem.* **276,** 32016–32021
69. Dennison, S. M., Greenfield, N., Lenard, J., and Lentz, B. R. (2002) *Biochemistry* **41,** 14925–14934
70. Chakrabartty, A., Kortemme, T., and Baldwin, R. L. (1994) *Protein Sci.* **3,** 843–852
71. Pace, C. N., and Scholtz, J. M. (1998) *Biophys. J.* **75,** 422–427
72. Rohl, C. A., Fiori, W., and Baldwin, R. L. (1999) *Proc. Natl. Acad. Sci. U. S. A.* **96,** 3682–3687
73. Zhang, Y. P., Lewis, R. N. A. H., Hodges, R. S., and McElhaney, R. N. (1995) *Biochemistry* **34,** 2362–2371
74. Killian, J. A., De Planque, M. R. R., Van der Wel, P. C. A., Salemink, I., De Kruijff, B., Greathouse, D. V., and Koeppe, R E., II (1998) *Pure Appl. Chem.* **70,** 75–82
75. Morein, S., Koeppe, R. E., Lindblom, G., de Kruijff, B., and Killian, J. A. (2000) *Biophys. J.* **78,** 2475–2485
76. Liu, F., Lewis, R. N. A. H., Hodges, R. S., and McElhaney, R. N. (2001) *Biochemistry* **40,** 760–768
77. Liu, F., Lewis, R. N. A. H., Hodges, R. S., and McElhaney, R. N. (2004) *Biochemistry* **43,** 3679–3687
78. van der Wel, P. C. A., Pott, T., Morein, S., Greathouse, D. V., Koeppe, R. E., and Killian, J. A. (2000) *Biochemistry* **39,** 3124–3133
79. Zhang, Y. P., Lewis, R. N. A. H., Hodges, R. S., and McElhaney, R. N. (2001) *Biochemistry* **40,** 474–482
80. Strandberg, E., Morein, S., Rijkers, D. T. S., Liskamp, R. M. J., van der Wel, P. C. A., and Killian, J. A. (2002) *Biochemistry* **41,** 7190–7198
81. Armstrong, R. T., Kushnir, A. S., and White, J. M. (2000) *J. Cell Biol.* **151,** 425–437
82. Owens, R. J., Burke, C., and Rose, J. K. (1994) *J. Virol.* **68,** 570–574
83. Pietschmann, T., Zentgraf, H., Rethwilm, A., and Lindemann, D. (2000) *J. Virol.* **74,** 4474–4482
84. Bos, E. C., Heijnen, L., Luytjes, W., and Spaan, W. J. (1995) *Virology* **214,** 453–463
85. Ragheb, J. A., and Anderson, W. F. (1994) *J. Virol.* **68,** 3207–3219
86. Saifee, O., Wei, L. P., and Nonet, M. L. (1998) *Mol. Biol. Cell* **9,** 1235–1252
87. Xu, Y. B., Zhang, F., Su, Z. L., Mcnew, J. A., and Shin, Y. K. (2005) *Nat. Struct. Mol. Biol.* **12,** 417–422